

🔍 SCALAR: Scale-wise Controllable Visual Autoregressive LeARning

Ryan Xu*, Dongyang Jin*, Yancheng Bai^{†‡}, Rui Lan,
Xu Duan, Lei Sun[†], and Xiangxiang Chu

Amap, Alibaba Group

ryansxu.00@gmail.com, {jindongyang.j, lr264907, xuxu.dx}@alibaba-inc.com,
{yancheng.byc, ally.sl, chuxiangxiang.cxx}@alibaba-inc.com

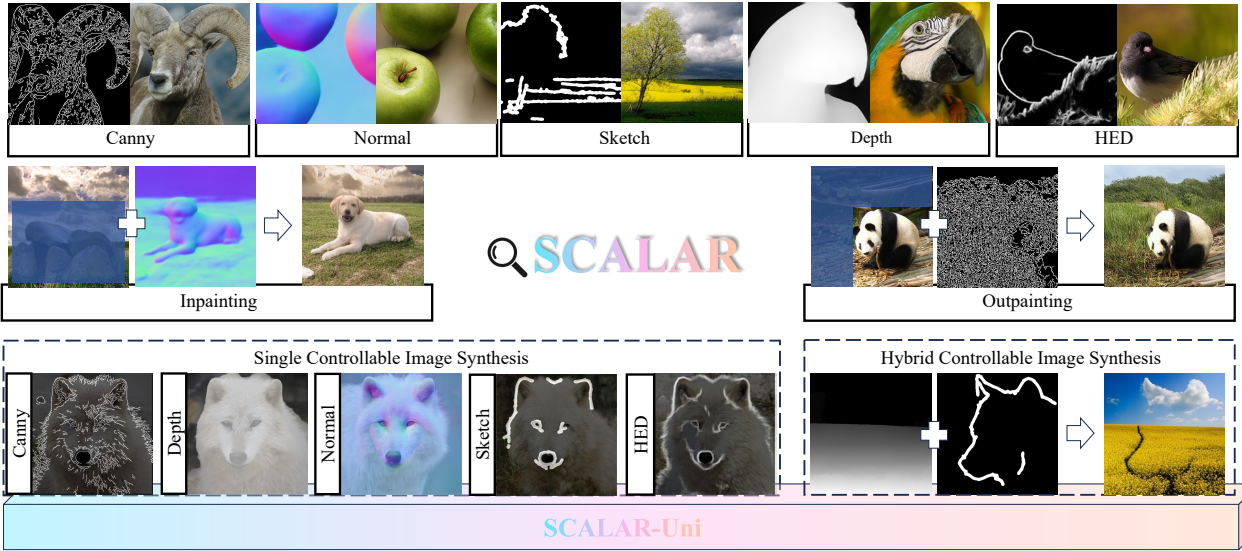


Figure 1. **SCALAR**, a novel controllable VAR method, achieves superior generation quality and control capabilities for various types of controllable signals (top row). It also exhibits robust zero-shot generalizability to tasks such as inpainting and outpainting (middle row). **SCALAR-Uni** further extends it by supporting multi-condition control within a unified model (bottom row).

Abstract

Controllable image synthesis, which enables fine-grained control over generated outputs, has emerged as a key focus in visual generative modeling. However, controllable generation remains challenging for Visual Autoregressive (VAR) models due to their hierarchical, next-scale prediction style. Existing VAR-based methods often suffer from inefficient control encoding and disruptive injection mechanisms that compromise both fidelity and efficiency. In this work, we present SCALAR, a controllable generation method based on VAR, incorporating a novel Scale-wise Conditional Decoding mechanism. SCALAR leverages a pretrained image encoder to extract semantic control signal encodings, which are projected into scale-specific representations and injected into the corresponding layers of the VAR backbone. This design provides persistent and struc-

turally aligned guidance throughout the generation process. Building on SCALAR, we develop SCALAR-Uni, a unified extension that aligns multiple control modalities into a shared latent space, supporting flexible multi-conditional guidance in a single model. Extensive experiments show that SCALAR achieves superior generation quality and control precision across various tasks. All the code will be released.

1. Introduction

Controllable image synthesis is a pivotal domain in visual generation, enabling the precise and nuanced creation of visual content according to specific user guidance. Recent advances in this field are currently dominated by two primary paradigms: Diffusion Models [11, 41] and Autoregressive Models (AR) [43, 45]. While diffusion-based methods [17, 32, 57] have achieved widespread success, the iterative denoising process is not inherently compatible with

*Equal contribution.

[†]Corresponding author.

[‡]Project Leader.

the sequential, token-based architecture of LLMs, which hinders the development of truly unified multimodal modeling [51, 61].

Visual Autoregressive (VAR) models [45], a leading approach within the autoregressive paradigm, offer a compelling path forward. By framing image synthesis as a next-scale prediction task, VAR-based models [9, 24, 44, 63] align naturally with LLM architectures and have demonstrated better inference efficiency and generative quality than both state-of-the-art diffusion models [31] and raster-scan-based autoregressive models [43]. Nevertheless, the capacity of VAR models for fine-grained control remains a significant and underexplored challenge. This challenge primarily stems from the unique hierarchical, scale-wise generation process, which presents a distinct paradigm from existing approaches: In diffusion models, control signals are applied globally to the denoising network at each step, whereas in traditional raster-scan AR models [16, 43], they are injected before each spatial token prediction.

Existing works on controllable Visual Autoregressive learning, notably CAR [53] and ControlVAR [20], deliver suboptimal performance. We attribute this bottleneck to two fundamental design flaws. First, they utilize complex and disruptive injection mechanisms; architectures with parallel branches [53] similar to ControlNet or joint control and image modeling schemes [20] not only incur substantial computational overhead but also implicitly disrupt the powerful generative capabilities of the pretrained backbone. Second, they often utilize lightweight convolutional networks or VQ-VAEs as control encoders, which have been proven to have a limited capacity in capturing rich spatial-semantic features [19, 62]. Consequently, their performance in both generation quality and control consistency trails behind even raster-scan AR models [21], highlighting a critical need for a control mechanism that is both efficient and fundamentally aligned with the native structure of VAR.

To this end, we present SCALAR, an effective controllable generation method based on VAR. Aligning with the more efficient paradigm [21], SCALAR injects control during the autoregressive decoding phase. Our approach is centered on a novel and simple **Scale-wise Conditional Decoding** mechanism. To be specific, we first employ a pretrained vision foundation model [6, 14, 29] to extract powerful, scale-agnostic control features that contain rich semantic information. These general features are then processed by scale-wise lightweight projection blocks—which maintain independent weights for each scale—to produce specialized **Control Signal Encodings**. Ultimately, SCALAR injects these tailored encodings directly into the hidden states of the VAR backbone’s layers, providing scale-wise persistent guidance throughout the next-scale prediction process. Building on our design, we extend SCALAR to a unified control version, SCALAR-uni. This extension incorporates a

Unified Control Alignment process that projects features from diverse control modalities into a common latent space, enabling seamless guidance of various condition types from a unified model.

The main contributions of this paper are as follows:

- We present SCALAR, a controllable generation method based on VAR that introduces a Scale-wise Conditional Decoding mechanism, explicitly designed to align with the next-scale prediction nature of VAR models.
- A Unified Control Alignment process is introduced to SCALAR-uni, enabling the various condition semantics guidance in controllable visual autoregressive learning.
- Extensive experiments on ImageNet demonstrate that **SCALAR** and **SCALAR-Uni** achieve exceptional generation quality and conditional consistency across all five conditional generation tasks (e.g., FID on Canny: **2.14** vs. 7.85; Depth: **3.09** vs. 4.19).

2. Related Work

2.1. Image Generation

Two dominant paradigms have emerged in image generation: diffusion models and AR models. Diffusion models synthesize images by iteratively denoising Gaussian noise, with DDPM [12] marking a major breakthrough. Subsequent work improves generation quality and efficiency [28, 36, 59] through advances in sampling strategies and latent-space modeling. They have become the backbone of text-to-image and text-to-video generation [15, 23, 37, 39, 60], typically using U-Net for denoising and CLIP or T5 for text conditioning via cross-attention. Recent models like DiT [30] replace U-Net with Transformer backbones, achieving strong performance. Despite their success, diffusion models remain computationally expensive, motivating exploration of more efficient alternatives such as autoregressive approaches.

In contrast, AR models formulate image synthesis as a sequence modeling task, predicting tokens step by step. Early works [48] focused on pixel-level generation. Building on the success of large language models [1, 47], emerging approaches adopt discrete quantizers such as VQ-VAE [49] and VQ-GAN [7] to convert image patches into discrete token indices, enabling next-token prediction over visual token sequences. Representative works such as LlamaGen [43] and Open-MAGVIT2 [22] adopt the LLaMA architecture [46], while AiM [16] explores the Mamba [8] as the autoregressive backbone. Among them, Visual Autoregressive Modeling (VAR) introduces a scalable next-scale prediction mechanism, which differs from traditional raster-scan AR methods. VAR-based models for class-to-image and text-to-image tasks [9, 24, 44, 45, 63] achieve image synthesis performance comparable to state-of-the-art diffusion models while offering significant computational

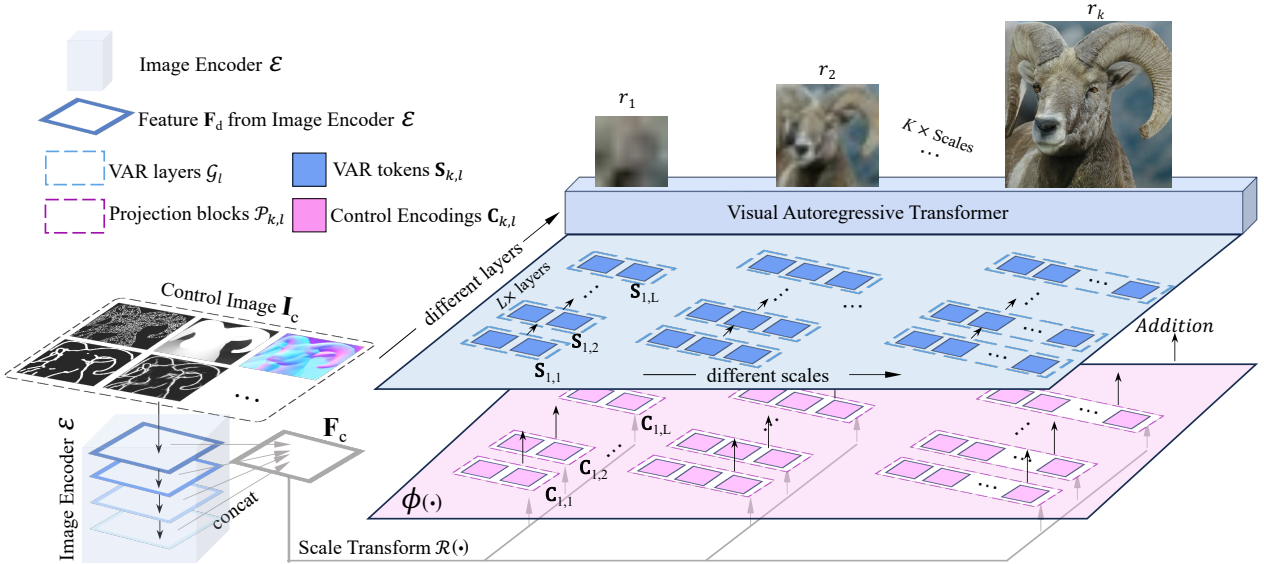


Figure 2. The framework of our **SCALAR** applies a next-scale paradigm adapted for VAR to design a Scale-wise Conditional Decoding mechanism (see Section 3.2 for details). The feature \mathbf{F}_c is obtained by concatenating four features \mathbf{F}_d extracted by the Image Encoder \mathcal{E} .

efficiency.

2.2. Controllable Image Generation

Conditional image generation, where the model is guided by external signals during the generative process, has become an active area of research. While early efforts leveraged class labels or attributes in GANs [25, 40] and VAEs [13, 56], recent advances focus on more fine-grained and flexible conditioning. In diffusion models, representative frameworks [27, 57] incorporate these signals via cross-attention or adapter-based modules, enabling high-quality, controllable generation without the need to fine-tune the full model. Follow-up works [17, 32, 34] further improve generalization and adaptability across diverse conditions and architectures.

In contrast, conditional generation for AR models has been far less explored. Existing works on controllable autoregressive learning are typically classified according to the guidance injection phase in autoregressive generation: pre-filling phase or decoding phase. Pre-filling-phase methods [20, 33] fill the control encodings into the initial sequence from the start. This approach increases the token sequence length, inflating the computational load, while the joint modeling scheme in ControlVAR [20] can disrupt the powerful capabilities of the pretrained backbone. Decoding-phase methods [21], which continuously inject control encodings throughout the step-by-step decoding, are simpler and more flexible. However, CAR [53] adopts parallel conditional decoding branches inspired by ControlNet, which introduces huge complexities when autoregressive

decoding. Notably, although VAR models generally outperform traditional AR models in image synthesis quality, these VAR-based controllable methods [20, 53] still underperform compared to raster-scan AR-based methods [21] in terms of control consistency and image quality. This gap indicates that the potential of VAR in controllable generation is yet to be fully explored. In this paper, we aim to develop a general and efficient method for controllable image generation based on VAR.

3. SCALAR

In this section, we present SCALAR, a simple and efficient method for controllable VAR. We first revisit the image generation with VAR. Next, we introduce Scale-wise Conditional Decoding. Then, we conduct several experiments to find the model architecture that yields the best generation quality and control consistency. Finally, we extend our approach to a unified version, SCALAR-Uni, with the proposed Unified Control Alignment.

3.1. Preliminary

Building upon the success of large language models [1, 47], visual autoregressive models adopt discrete quantizers such as VQVAE to convert image patches into index-wise tokens, enabling image generation via next-step prediction over visual token sequences. Among them, VAR introduces a scalable next-scale prediction mechanism, which generates images in a coarse-to-fine manner across spatial resolutions. VAR-based class-to-image (c2i) [45] and text-to-image (t2i) [9, 24, 44, 63] models achieve image synthesis

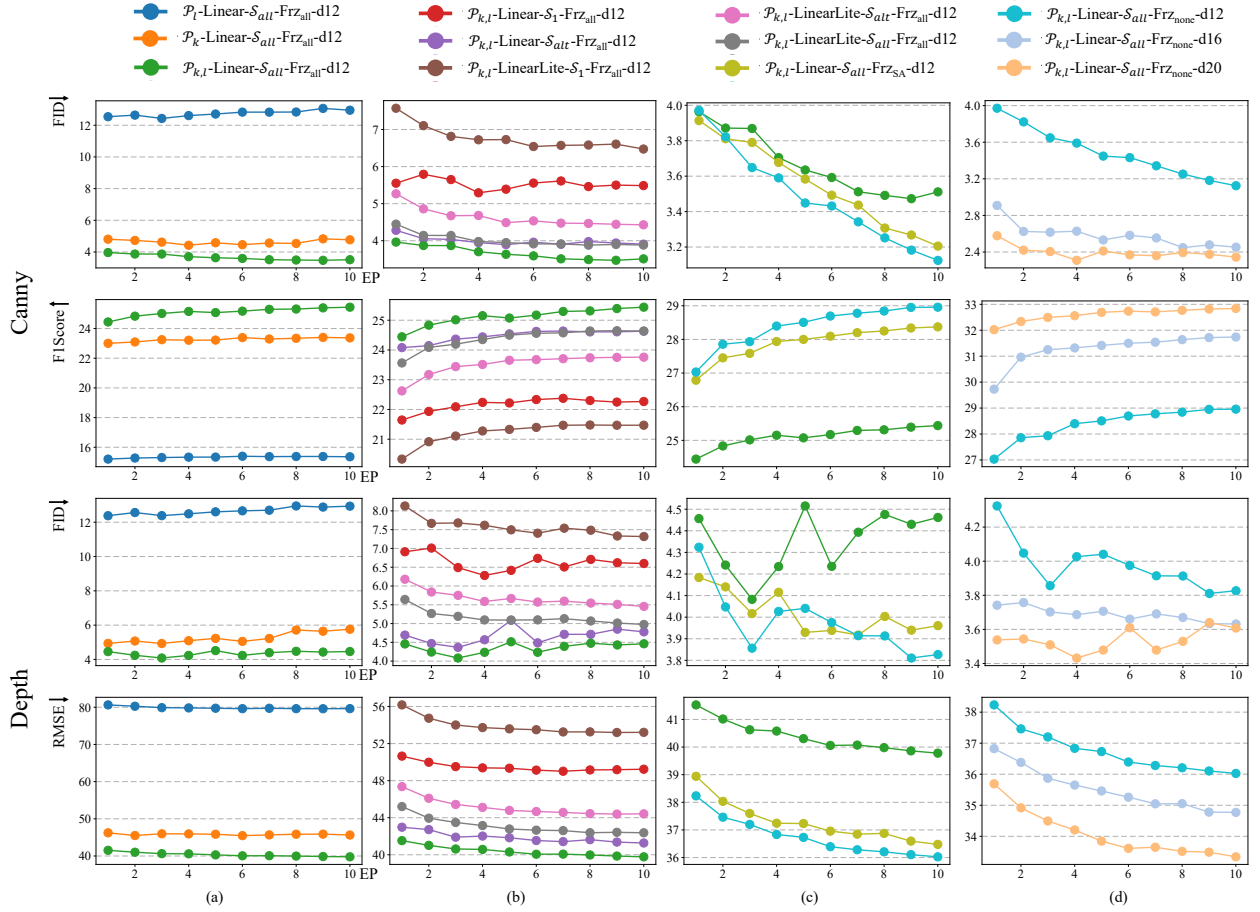


Figure 3. (a) Comparison of parameter sharing for projection blocks ($\mathcal{P}_{k,l}$, \mathcal{P}_k , and \mathcal{P}_l). (b) Comparison of various injection layers set (\mathcal{S}_1 , \mathcal{S}_{alt} , and \mathcal{S}_{all}) with different structures of projection block (**Linear** and **LinearLite**). (c) Comparison of different parameter-efficient training strategies (Frz_{none}, Frz_{SA}, and Frz_{all}). (d) Impacts of scaling up the depth of VAR backbone (VAR-d12, d16, and d20).

performance comparable to state-of-the-art diffusion models, while reducing computational cost.

The core idea of the VAR model lies in next-scale prediction, which contrasts with traditional raster-scan AR models based on next-token prediction. While conventional AR models generate images token by token along a flattened pixel sequence, this formulation suffers from mathematical inconsistencies and often leads to structural degradation, especially in highly structured images. In contrast, VAR avoids these issues by operating at the level of token maps, predicting the image progressively across multiple scales. Starting from a coarse 1×1 token map r_1 , it autoregressively generates a sequence of higher-resolution token maps (r_2, \dots, r_K) , each representing a finer level of detail. The overall generation process is formulated as:

$$p(r_1, r_2, \dots, r_K) = \prod_{k=1}^K p(r_k \mid r_{<k}), \quad (1)$$

where $r_k \in [V]^{h_k \times w_k}$ represents the token map at scale k ,

with dimensions h_k and w_k , conditioned on previous maps $r_{<k}$. Each token in r_k is an index from the VQVAE codebook V , which is trained through multi-scale quantization and shared across scales. A standard cross-entropy loss is used to supervise VAR, defined as:

$$\mathcal{L}_{CE} = \mathbb{E}_{r_k \sim p(r_k)} [-\log p_\theta(r_k \mid r_{<k})]. \quad (2)$$

The loss is applied at each scale to train the model to predict finer token maps conditioned on coarser ones.

3.2. Scale-wise Conditional Decoding

The generation process in autoregressive models is bifurcated into two phases: pre-filling and decoding. In SCALAR, we diverge from the conditional pre-filling way [20, 33], which relies on a distinct initial conditioning filling step. We adopt a simpler conditional decoding strategy [21, 53]. This design integrates the control signal directly and continuously throughout the decoding process. The scale-autoregressive nature of VARs poses distinct re-

quirements for how control signals are applied across the generative hierarchy; guidance must be present and adapted at each scale. SCALAR achieves this by injecting the control signal into a predefined subset of layers, indexed by $l \in \mathcal{S}$. Formally, the operation at each layer is expressed as:

$$\mathbf{S}'_{k,l} = \mathcal{G}_l(\mathbf{S}_{k,l} + \mathbf{C}_{k,l}), \quad (3)$$

where \mathcal{G}_l represents the l -th layer of the GPT-style decoder transformer, $\mathbf{S}_{k,l}$ and $\mathbf{S}'_{k,l}$ denote the input and output sequence of image tokens at layer l for scale k , and $\mathbf{C}_{k,l}$ is the corresponding control signal encoding sequence injected at that same layer and scale. The set $\mathcal{S} \subseteq \{0, \dots, L-1\}$ contains the indices of the layers targeted for injection, where L is the total depth of the decoder \mathcal{G} .

Control Signal Encoding $\mathbf{C}_{k,l}$. We employ a pretrained vision foundation model [6, 14, 29] as our universal control signal encoder. Its inherent understanding of rich visual semantics, learned via large-scale self-supervision, provides a powerful and robust feature extractor for diverse control conditions. To leverage the hierarchical features within the encoder [2], the control representation \mathbf{F}_c is formed by concatenating features from the i -th layers of the encoder \mathcal{E} . It can be expressed as:

$$\mathbf{F}_c = \mathcal{C} \left(\left. \mathcal{E}_i(\mathbf{I}_c) \right|_{i \in \mathcal{I}} \right), \quad (4)$$

where $\mathcal{E}_i(\cdot)$ is the feature from the i -th layer of the encoder, $\mathcal{C}(\cdot)$ represents the concatenation operation and \mathcal{I} is the set of indices for the selected layers. The resulting scale-agnostic feature \mathbf{F}_c is then tailored for injection into scale k and layer l of our Scale-wise Conditional Decoding process

$$\mathbf{C}_{k,l} = \phi_{k,l}(\mathbf{F}_c) = \mathcal{P}_{k,l}(\mathcal{R}_{h_k, w_k}(\mathbf{F}_c)), \quad (5)$$

where \mathcal{R}_{h_k, w_k} denotes transforming the features to the target spatial size (h_k, w_k) of scale k . Subsequently, a conditional projection block $\mathcal{P}_{k,l}$ maps to the final control signal encoding $\mathbf{C}_{k,l}$.

3.3. Exploring Controlled Architectural Design

We explore several strategies to determine the optimal architecture for SCALAR. Our primary goal is to identify the most effective designs for encoding and injecting control signals into the VAR’s generative process. We focus our experiments on the following key architectural observations:

- **Parameter Sharing of $\mathcal{P}_{k,l}$.** The control signal is injected via projection blocks. We investigate different parameter-sharing strategies for these layers. Specifically, we explore whether the projection weights should be: (i) unique for each transformer layer at each scale, marked as $\mathcal{P}_{k,l}$, (ii) shared across all layers, marked as \mathcal{P}_k , or (iii) shared across all scales, marked as \mathcal{P}_l .

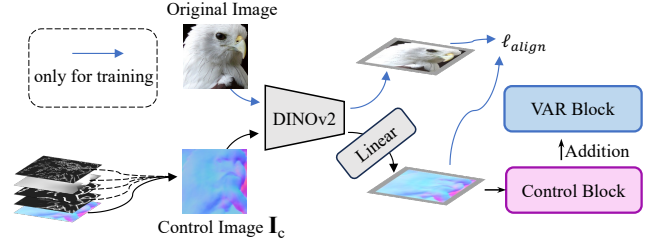


Figure 4. Our SCALAR-Uni, A unified multi-condition control method. Building on SCALAR, we introduce unified control alignment to map diverse control features into a common, modality-agnostic latent space. During training, control images are randomly sampled with equal probability.

- **Projection Blocks $\mathcal{P}_{k,l}$ and Injection Layers Set \mathcal{S} .** By default, $\mathcal{P}_{k,l}$ is a single linear layer, which can be parameter-intensive, especially when the injection set \mathcal{S} is large. We explore two main aspects:
 - **Structure of $\mathcal{P}_{k,l}$:** We compare (i) **Linear**: a standard linear layer against (ii) **LinearLite**: a more parameter-efficient bottleneck structure, which consists of two linear layers that first squeeze the channel dimension and then expand it back.
 - **Injection Set \mathcal{S} :** We investigate how the density of control signal injection affects performance by testing three configurations for \mathcal{S} : (i) injecting only into the first layer $\mathcal{S}_1 = \{1\}$, (ii) injecting into alternating layers $\mathcal{S}_{\text{alt}} = \{1, 3, 5, \dots, L-1\}$, and (iii) injecting into all layers $\mathcal{S}_{\text{all}} = \{1, 2, 3, \dots, L\}$.
- **Parameter-Efficient Training.** We analyze various training strategies to evaluate the trade-off between performance and the number of trainable parameters. Specifically, we compare: (i) **Frz_{none}**: fine-tuning all VAR parameters, (ii) **Frz_{SA}**: freeze all self-attention layers of VAR, and (iii) **Frz_{all}**: freeze all VAR parameters.

For all comparisons above, we train VAR-d12 models on ImageNet 256 × 256 with batch size 512. We train models with the above changes and compare them on Fréchet Inception Distance (FID), Inception Score (IS), Root Mean Square Error (RMSE, conditioned on Depth), and F1-Score (conditioned on Canny). As shown in Figure 3(a) and (b), the optimal configuration employs projection blocks with scale-wise parameters for each block ($\mathcal{P}_{k,l}$), uses a standard linear layer (**Linear**), and injects the control signal into all layers (\mathcal{S}_{all}). Figure 3(c) shows that freezing backbone parameters causes a significant reduction of control performance. In Figure 3(d), scaling up depth of VAR helps performance. Accordingly, we adopt the best combination of settings ($\mathcal{P}_{k,l}$ -**Linear**- \mathcal{S}_{all} -**Frz_{none}**) for our final SCALAR model to achieve the best performance. Further analysis details about Figure 3 are provided in the **Supplementary Material**.

Table 1. Quantitative results of conditional image generation on ImageNet [5]. Values marked with \sim are estimated from histograms in the corresponding paper. Cells highlighted with indicate the best performance for each setting.

Type	Method	Model	Canny			Depth			Normal			HED			Sketch		
			FID \downarrow	IS \uparrow	F1-Score \uparrow	FID \downarrow	IS \uparrow	RMSE \downarrow	FID \downarrow	IS \uparrow	RMSE \downarrow	FID \downarrow	IS \uparrow	SSIM \uparrow	FID \downarrow	IS \uparrow	F1-Score \uparrow
Diff.	T2IAdapter [26]	-	~10.2	~157	-	~9.9	~134	-	~9.5	~143	-	~9.3	~142	-	~16.2	~156	-
	ControlNet [58]	-	~11.6	~173	-	~9.2	~150	-	~8.9	~155	-	~8.6	~150	-	~15.3	~163	-
AR	ControlAR [21]	AiM-L	9.66	-	30.36	7.39	-	35.01	-	-	-	-	-	-	-	-	-
		LlamaGen-B	10.64	-	34.15	6.67	-	32.41	-	-	-	-	-	-	-	-	-
		LlamaGen-L	7.69	-	34.91	4.19	-	31.11	-	-	-	-	-	-	-	-	-
VAR	ControlVAR [20]	VAR-d12	~35.2	~44	-	~26.7	52	-	~25.3	~55	-	-	-	-	-	-	-
		VAR-d16	~16.2	~80	-	~13.8	92	-	~14.2	~89	-	-	-	-	-	-	-
		VAR-d20	~13.0	~94	-	~13.4	98	-	~12.8	~100	-	-	-	-	-	-	-
		VAR-d24	~15.7	~100	-	~12.5	125	-	~11.8	~123	-	-	-	-	-	-	-
		VAR-d30	7.85	160.0	-	6.50	180.5	-	6.20	172.0	-	-	-	-	-	-	-
	CAR [53]	VAR-d16	~12.8	~85	-	~10.8	~95	-	~11.0	~98	-	~9.8	~102	-	~13.2	~83	-
		VAR-d20	~10.2	~125	-	~8.0	~135	-	~8.8	~138	-	~7.2	~144	-	~11.2	~118	-
		VAR-d24	~9.0	~155	-	~7.0	~165	-	~7.5	~168	-	~6.5	~176	-	~10.0	~143	-
		VAR-d30	8.30	167.3	-	6.90	178.6	-	6.60	175.9	-	5.60	182.2	-	10.20	161.6	-
	SCALAR (Ours)	VAR-d12	3.12	191.3	28.96	3.83	233.3	36.03	3.76	225.7	28.14	2.62	189.1	74.93	4.55	229.6	76.60
		VAR-d16	2.45	237.7	31.74	3.63	285.8	34.77	3.70	279.5	27.64	1.97	222.5	76.37	4.51	292.4	77.03
		VAR-d20	2.34	254.3	32.84	3.61	301.3	33.34	3.51	300.9	27.57	1.81	240.4	76.74	4.22	312.7	77.43
	SCALAR-Uni (Ours)	VAR-d24	2.14	261.8	33.14	3.09	306.9	33.13	3.09	307.2	27.45	1.72	244.2	76.98	3.57	315.5	77.58

3.4. Unified Control Alignment

Benefiting from the architectural simplicity of SCALAR, extending it to manage multiple conditions simultaneously requires addressing a key challenge: the control features extracted for different modalities (e.g., Canny edges, depth maps) reside in distinct and potentially incompatible feature spaces. As shown in Figure 4, we propose a unified version, **SCALAR-Uni**. The core idea is to map disparate control features into a common, modality-agnostic latent space. We utilize the image feature space itself as the target for this alignment, as it offers a rich and universal representation of visual concepts. We enforce this alignment by introducing an auxiliary loss term during training, which minimizes the L2 distance between the projected control representations and the corresponding image features:

$$\begin{aligned} \mathcal{L}_{\text{align}} &= \|\mathcal{F}_{\text{align}}(\mathbf{F}_c) - \mathbf{F}_{\text{img}}\|_2^2 \\ &= \left\| \mathcal{F}_{\text{align}}(\mathbf{F}_c) - \mathcal{C} \left(\mathcal{E}_i(\mathbf{I}_{\text{img}}) \right) \right\|_2^2 \end{aligned} \quad (6)$$

where \mathbf{I}_{img} represents the corresponding image for control signal, $\mathcal{F}_{\text{align}}$ represents a lightweight alignment module, implemented as a linear layer, learning to project the initial control representation \mathbf{F}_c into this shared image feature space. The total training loss of SCALAR-Uni can be formulated as:

$$\mathcal{L} = \mathcal{L}_{\text{CE}} + \lambda \mathcal{L}_{\text{align}}, \quad (7)$$

where λ is a constant that regulates the alignment loss.

4. Results

4.1. Experimental Setup

Dataset. We conduct experiments on the ImageNet-256 [5], using all 50K images from the validation set for evaluation. To assess the controllable generation capability of our model, we consider five types of conditions: Canny [4], Depth [35], Normal [50], HED [52], and Sketch [42].

Training Details. We extract four features from the Image Encoder \mathcal{E} at the layers specified by the index set $\mathcal{I} = \{d - 1 - k \cdot \lfloor d/4 \rfloor \mid k \in \{0, 1, 2, 3\}\}$. We use DINOv2 [29] as the Image Encoder for its strong representations and scalability. As shown in Table 1, we use pretrained VARs with depths of 12, 16, 20, and 24, adopting DINOv2-S for 12 and DINOv2-B otherwise. Following previous works [18, 58], the control block is zero-initialized. Our SCALAR and SCALAR-Uni are trained for 10 epochs with the AdamW optimizer on 8 NVIDIA H20 GPUs. For SCALAR-Uni, we sample different control conditions with equal probability.

Evaluation Metrics. We mainly employ two metrics: conditional consistency and image generation quality. We evaluate the conditional consistency by calculating the similarity between the input condition images and the extracted condition images from the generated images. Specifically, we use F1-Score to assess the similarity of Canny and Sketch, Root Mean Square Error (RMSE) for Normal and Depth, and Structural Similarity Index Measure (SSIM) for HED. For image generation quality, we use Fréchet Inception Distance (FID) [10] and Inception Score (IS) [38].

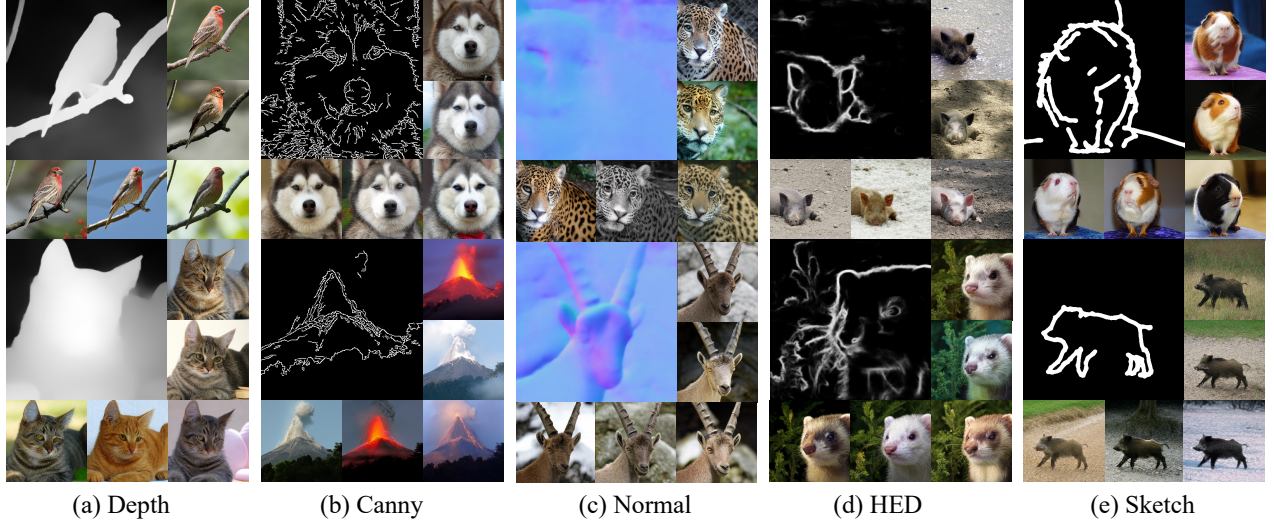


Figure 5. Visual results generated by SCALAR.

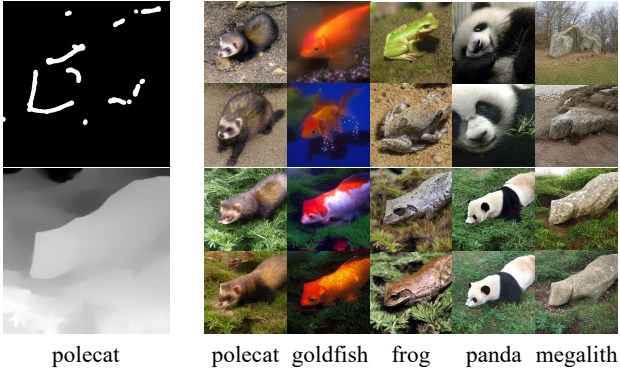


Figure 6. Visualization of controllable image synthesis with SCALAR by changing class labels (e.g., “polecat” \rightarrow “goldfish”).

4.2. Experimental Results

We evaluate the controllable generation performance of our proposed SCALAR and SCALAR-Uni on the ImageNet [5]. As shown in Table 1, we compute both conditional consistency and image generation quality for the images generated by SCALAR and SCALAR-Uni. Furthermore, we compare our approach with existing controllable generation methods, including diffusion-based models [26, 58], raster-scan AR models [21], and VAR-based methods [20, 53].

Results for SCALAR. Results show that SCALAR consistently outperforms existing methods in image generation quality, achieving superior FID and IS scores. Notably, even SCALAR-d12 achieves better FID compared to ControlAR with LlamaGen-L, while VAR-d12 uses only **50.1%** of the parameters of LlamaGen-L (e.g., FID on Canny: **3.12** vs. 7.85; Depth: **3.83** vs. 4.19). In terms of conditional consistency, SCALAR also demonstrates competitive performance against other State-of-the-Art (SoTA) methods.

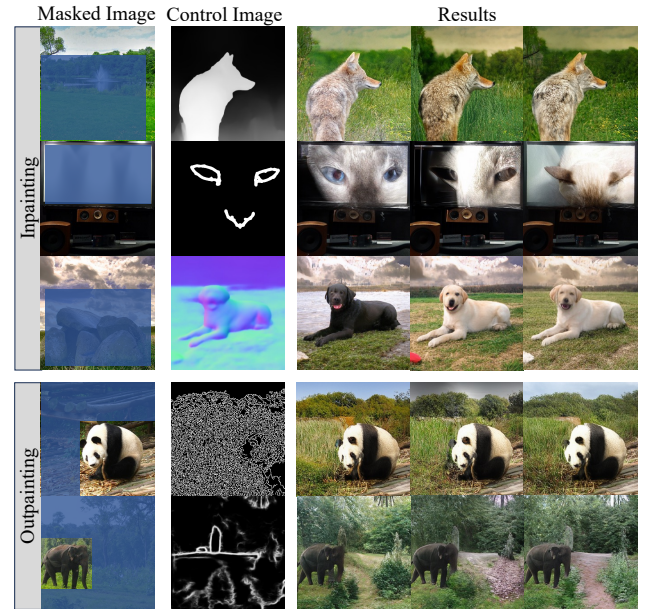


Figure 7. Visualization of zero-shot controllable image synthesis with SCALAR, including inpainting and outpainting. From top to bottom, Depth, Sketch, Normal, Canny, and HED are used as control image inputs.

Moreover, as the depth of the underlying VAR increases, both the generation quality and the conditional consistency of SCALAR steadily improve. Qualitative visualizations of the generated results are shown in Figure 5. Besides, SCALAR also demonstrates strong generalization by synthesizing an object of the target class while adhering to the spatial structure of the source control image, even when the label and control structure are inconsistent, as illustrated in Figure 6.

Zero-shot Controllable In- and Outpainting. SCALAR

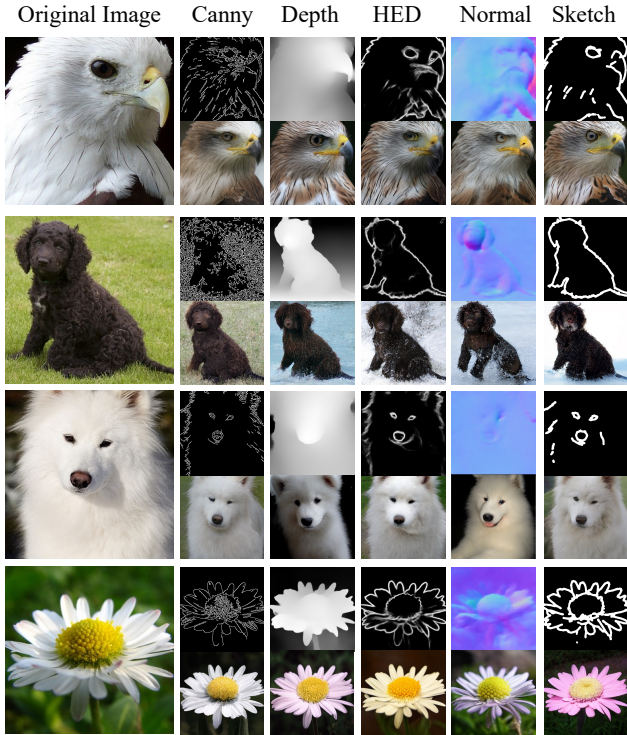


Figure 8. Visual results generated by our unified multi-condition control method SCALAR-Uni under varying control conditions.

is tested. For in-painting and out-painting, we teacher-force ground-truth tokens outside the control-image-guided mask. The model is required to generate tokens only within the masked region. During this process, class label information from the control images is also injected. As shown in Figure 7, without any retraining, SCALAR achieves strong performance on these downstream tasks, further validating its generalization capability

Results for SCALAR-Uni. Compared to other SoTA methods [20, 21, 26, 53, 58], SCALAR-Uni demonstrates clear advantages in image generation quality while maintaining high conditional consistency. When compared to SCALAR, SCALAR-Uni shows a slight drop in both generation quality and consistency, which may be attributed to the need to accommodate multiple control conditions, thereby reducing the effective training data per condition. Overall, SCALAR-Uni exhibits strong performance and generalization as a unified framework for multi-condition controllable generation. More visualization details can be found in Figure 8.

Zero-shot Hybrid Controllable Synthesis. SCALAR-Uni is tested. Given the Unified Control Alignment strategy of SCALAR-Uni, we consider two different categories of control images as inputs (e.g., Depth+Sketch, Normal+Canny, etc.). In addition to the corresponding control images, the class conditions of both inputs are also fed into SCALAR-

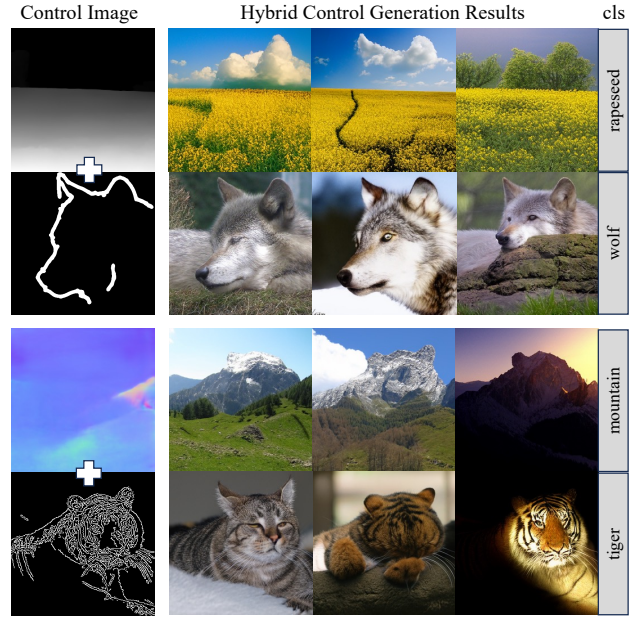


Figure 9. Visualization of zero-shot hybrid controllable image synthesis with SCALAR-Uni, combining two control types (e.g., Depth+Sketch) to generate images with both characteristics. Different class-condition injections are applied for each control pair.

Uni. As in the zero-shot tasks of SCALAR, no retraining is conducted. As shown in Figure 9, SCALAR-Uni successfully combines different control types and generates high-quality images with the characteristics of both controls. This experiment demonstrates the strong generalization ability of SCALAR-Uni, where the Unified Control Alignment effectively maps diverse control features into a common, modality-agnostic latent space.

4.3. Ablation Study

Classify Free Guidance. Given the same control image, we further visualize the results generated with different guidance scales in Figure 10. We observe that both excessively low and high guidance scales result in lower-quality images. Therefore, we set the guidance scale to 4.0 in our experiments.

Ablations on Image Encoder \mathcal{E} . In Table 2, we conduct experiments using different image encoders (or pretraining schemes) towards different controls on ImageNet [5], including Canny and Depth. Firstly, unlike previous approaches [21, 53], SCALAR and SCALAR-Uni adopt frozen image encoders [6, 14, 29] to preserve the robust features obtained from large-scale self-supervised pretraining. In addition, inspired by prior work [3, 54, 55], we extract multi-layer features including intermediate layers, instead of relying solely on the final output, which improves image generation quality while maintaining control consis-



Figure 10. Visualization of images generated with different guidance scales. All images at the same position are generated by the same random seed.

tency. As shown in Table 2 (c) to (g), DINOv2 [29] outperforms other pretrained vision models such as ViT [6] and SAM [14]. Furthermore, comparing (d), (e), (c), and (g) indicates that increasing the scale of the image encoder significantly boosts performance under the same backbone. Considering the trade-off between parameter size and effectiveness, we use DINOv2-s for the d12 architecture and DINOv2-b for all other settings. Finally, the comparison from (g) to (j) demonstrates that deeper VAR networks lead to further improvements in both generation quality and control accuracy, suggesting that deeper models can better exploit visual representations.

Ablations on Unified Control Alignment. We evaluate our SCALAR-Uni under different depths (d12, d16, d20, and d24) on ImageNet [5]. While the model is trained with five types of control conditions, the effectiveness of Unified Control Alignment is validated only on Canny and Depth. As shown in Table 3, without the Unified Control Alignment, **SCALAR-Uni** is equivalent to **SCALAR** trained with mixed supervision across the five control types. Thanks to the strong general visual representation capability of DINOv2, **SCALAR** can effectively capture the differences across modalities and achieve preliminary alignment of multi-modal control signals. After incorporating Unified Control Alignment, **SCALAR-Uni** consistently outperforms **SCALAR** across different network depths in both image generation quality and control consistency. Results in Table 3 demonstrate that **SCALAR-Uni**, constructed by integrating **SCALAR** with Unified Control Alignment, offers a simple and effective solution for controllable image generation under diverse conditions.

5. Conclusion and Future Work

Conclusion. In this work, we propose SCALAR, a controllable generation method based on VAR that introduces a Scale-wise Conditional Decoding mechanism adapted for the hierarchical nature of VAR models. By leveraging a pretrained image encoder to extract semantically

Table 2. Ablation of Image Encoder \mathcal{E} and the backbone depth of VAR. ■ cells mark Image Encoder parameters comparable to CAR [53] / ControlAR [21], with a smaller backbone.

Index	Image Encoder \mathcal{E}	Para. of \mathcal{E}	Backbone	Canny			Depth			
				FID \downarrow	IS \uparrow	F1-Score \uparrow	FID \downarrow	IS \uparrow	RMSE	
ControlAR	(a)	21.8M	AiM-L	9.66	-	30.36	7.39	-	35.01	
			LlamaGen-B	10.64	-	34.15	6.67	-	32.41	
			LlamaGen-L	7.69	-	34.91	4.19	-	31.11	
CAR	(b)	21.2M	VAR-d16	-12.8	-85	-	-10.8	-95	-	
			VAR-d30	8.30	167.3	-	6.90	178.6	-	
	(c)	DINOv2-S	22.1M	VAR-d12	3.12	191.3	28.96	3.83	233.3	36.03
	(d)	ViT-S	21.8M	VAR-d12	4.34	189.5	24.19	5.01	230.9	42.00
	(e)	VIT-B	86.4M	VAR-d12	4.23	193.3	25.98	4.83	237.6	40.77
	(f)	SAM-B	89.6M	VAR-d12	6.13	165.1	28.41	5.72	210.0	40.41
	(g)	DINOv2-B	86.6M	VAR-d12	2.95	188.5	29.37	3.68	230.6	35.50
	(h)	DINOv2-B	86.6M	VAR-d16	2.45	237.7	31.74	3.63	285.8	34.77
	(i)	DINOv2-B	86.6M	VAR-d20	2.34	254.3	32.84	3.61	301.3	33.34
	(j)	DINOv2-B	86.6M	VAR-d24	2.14	261.8	33.14	3.09	306.9	33.13

Table 3. Ablations on SCALAR-Uni regarding the unified control alignment \mathcal{L}_{align} .

Model	Canny			Depth		
	FID \downarrow	IS \uparrow	F1-Score \uparrow	FID \downarrow	IS \uparrow	RMSE \downarrow
SCALAR-Uni-d12	3.31	207.4	27.52	4.21	231.5	38.57
↑ w/o \mathcal{L}_{align} in eq. 6	3.73	198.7	26.35	4.40	217.6	40.79
SCALAR-Uni-d16	2.78	262.4	30.76	3.73	294.1	37.24
↑ w/o \mathcal{L}_{align} in eq. 6	2.88	235.0	30.23	4.09	254.6	37.85
SCALAR-Uni-d20	2.64	276.9	31.68	3.69	310.1	37.12
↑ w/o \mathcal{L}_{align} in eq. 6	2.84	247.3	31.50	3.74	272.7	36.88

rich control features and injecting them into scale-specific layers, SCALAR enables persistent and structured guidance throughout the generation process. Our extension, SCALAR-Uni, further supports unified multi-conditional control. We hope our findings will inspire further research on controllable generation within Visual Autoregressive models and encourage the exploration of scale-aware design in future generative methods.

Future Work. (1) To align with the next-scale paradigm in VAR, we directly inject control features extracted from the image encoder into corresponding scales after resizing them via bilinear interpolation. While simple to implement, this approach is relatively coarse and lacks fine-grained semantic alignment, which may limit the further improvement of SCALAR’s controllability. This issue is worth further study. (2) Due to resource constraints, our SCALAR is currently evaluated only on c2i tasks using the ImageNet, where it demonstrates strong performance in both generation quality and controllability. In future work, we plan to extend SCALAR to controllable t2i generation tasks and validate its effectiveness on diverse text-image paired datasets. (3) SCALAR successfully combines the powerful generation capabilities of VAR with a simple and effective control injection mechanism. We are excited to inspire related tasks (e.g., image editing).

References

- [1] Josh Achiam, Steven Adler, Sandhini Agarwal, Lama Ahmad, Ilge Akkaya, Florencia Leoni Aleman, Diogo Almeida, Janko Altenschmidt, Sam Altman, Shyamal Anadkat, et al. Gpt-4 technical report. *arXiv preprint arXiv:2303.08774*, 2023. [2](#), [3](#)
- [2] Daniel Bolya, Po-Yao Huang, Peize Sun, Jang Hyun Cho, Andrea Madotto, Chen Wei, Tengyu Ma, Jiale Zhi, Jathushan Rajasegaran, Hanoona Rasheed, et al. Perception encoder: The best visual embeddings are not at the output of the network. *arXiv preprint arXiv:2504.13181*, 2025. [5](#)
- [3] Daniel Bolya, Po-Yao Huang, Peize Sun, Jang Hyun Cho, Andrea Madotto, Chen Wei, Tengyu Ma, Jiale Zhi, Jathushan Rajasegaran, Hanoona Rasheed, et al. Perception encoder: The best visual embeddings are not at the output of the network. *arXiv preprint arXiv:2504.13181*, 2025. [8](#)
- [4] John Canny. A computational approach to edge detection. *IEEE Transactions on pattern analysis and machine intelligence*, (6):679–698, 1986. [6](#)
- [5] Jia Deng, Wei Dong, Richard Socher, Li-Jia Li, Kai Li, and Li Fei-Fei. Imagenet: A large-scale hierarchical image database. In *2009 IEEE conference on computer vision and pattern recognition*, pages 248–255. Ieee, 2009. [6](#), [7](#), [8](#), [9](#)
- [6] Alexey Dosovitskiy. An image is worth 16x16 words: Transformers for image recognition at scale. *arXiv preprint arXiv:2010.11929*, 2020. [2](#), [5](#), [8](#), [9](#)
- [7] Patrick Esser, Robin Rombach, and Bjorn Ommer. Taming transformers for high-resolution image synthesis. In *Proceedings of the IEEE/CVF conference on computer vision and pattern recognition*, pages 12873–12883, 2021. [2](#)
- [8] Albert Gu and Tri Dao. Mamba: Linear-time sequence modeling with selective state spaces. *arXiv preprint arXiv:2312.00752*, 2023. [2](#)
- [9] Jian Han, Jinlai Liu, Yi Jiang, Bin Yan, Yuqi Zhang, Zehuan Yuan, Bingyue Peng, and Xiaobing Liu. Infinity: Scaling bit-wise autoregressive modeling for high-resolution image synthesis. In *Proceedings of the Computer Vision and Pattern Recognition Conference*, pages 15733–15744, 2025. [2](#), [3](#)
- [10] Martin Heusel, Hubert Ramsauer, Thomas Unterthiner, Bernhard Nessler, and Sepp Hochreiter. Gans trained by a two time-scale update rule converge to a local nash equilibrium. *Advances in neural information processing systems*, 30, 2017. [6](#)
- [11] Jonathan Ho, Ajay Jain, and Pieter Abbeel. Denoising diffusion probabilistic models. *Advances in neural information processing systems*, 33:6840–6851, 2020. [1](#)
- [12] Jonathan Ho, Ajay Jain, and Pieter Abbeel. Denoising diffusion probabilistic models. *Advances in neural information processing systems*, 33:6840–6851, 2020. [2](#)
- [13] Diederik P Kingma, Max Welling, et al. Auto-encoding variational bayes, 2013. [3](#)
- [14] Alexander Kirillov, Eric Mintun, Nikhila Ravi, Hanzi Mao, Chloe Rolland, Laura Gustafson, Tete Xiao, Spencer Whitehead, Alexander C Berg, Wan-Yen Lo, et al. Segment anything. In *Proceedings of the IEEE/CVF international conference on computer vision*, pages 4015–4026, 2023. [2](#), [5](#), [8](#), [9](#)
- [15] Rui Lan, Yancheng Bai, Xu Duan, Mingxing Li, Lei Sun, and Xiangxiang Chu. Flux-text: A simple and advanced diffusion transformer baseline for scene text editing. *arXiv preprint arXiv:2505.03329*, 2025. [2](#)
- [16] Haopeng Li, Jinyue Yang, Kexin Wang, Xuerui Qiu, Yuhong Chou, Xin Li, and Guoqi Li. Scalable autoregressive image generation with mamba. *arXiv preprint arXiv:2408.12245*, 2024. [2](#)
- [17] Ming Li, Taojiannan Yang, Huafeng Kuang, Jie Wu, Zhaoning Wang, Xuefeng Xiao, and Chen Chen. Controlnet++: Improving conditional controls with efficient consistency feedback. *arXiv preprint arXiv:2404.07987*, 2024. [1](#), [3](#)
- [18] Ming Li, Taojiannan Yang, Huafeng Kuang, Jie Wu, Zhaoning Wang, Xuefeng Xiao, and Chen Chen. Controlnet++: Improving conditional controls with efficient consistency feedback. In *European Conference on Computer Vision*, pages 129–147. Springer, 2024. [6](#)
- [19] Xiang Li, Kai Qiu, Hao Chen, Jason Kuen, Jiuxiang Gu, Bhiksha Raj, and Zhe Lin. Imagefolder: Autoregressive image generation with folded tokens. *arXiv preprint arXiv:2410.01756*, 2024. [2](#)
- [20] Xiang Li, Kai Qiu, Hao Chen, Jason Kuen, Zhe Lin, Rita Singh, and Bhiksha Raj. Controlvar: Exploring controllable visual autoregressive modeling. *arXiv preprint arXiv:2406.09750*, 2024. [2](#), [3](#), [4](#), [6](#), [7](#), [8](#)
- [21] Zongming Li, Tianheng Cheng, Shoufa Chen, Peize Sun, Haocheng Shen, Longjin Ran, Xiaoxin Chen, Wenyu Liu, and Xinggang Wang. Controllar: Controllable image generation with autoregressive models. *arXiv preprint arXiv:2410.02705*, 2024. [2](#), [3](#), [4](#), [6](#), [7](#), [8](#), [9](#)
- [22] Zhuoyan Luo, Fengyuan Shi, Yixiao Ge, Yujiu Yang, Limin Wang, and Ying Shan. Open-magvit2: An open-source project toward democratizing auto-regressive visual generation. *arXiv preprint arXiv:2409.04410*, 2024. [2](#)
- [23] Jingzhe Ma, Haoyu Luo, Zixu Huang, Dongyang Jin, Rui Wang, Johann A Briffa, Norman Poh, and Shiqi Yu. Passersby-anonymizer: Safeguard the privacy of passersby in social videos. In *2024 IEEE International Joint Conference on Biometrics (IJCB)*, pages 1–10. IEEE, 2024. [2](#)
- [24] Xiaoxiao Ma, Mohan Zhou, Tao Liang, Yalong Bai, Tiejun Zhao, Huaian Chen, and Yi Jin. Star: Scale-wise text-to-image generation via auto-regressive representations. *arXiv preprint arXiv:2406.10797*, 2024. [2](#), [3](#)
- [25] Mehdi Mirza and Simon Osindero. Conditional generative adversarial nets. *arXiv preprint arXiv:1411.1784*, 2014. [3](#)
- [26] Chong Mou, Xintao Wang, Liangbin Xie, Yanze Wu, Jian Zhang, Zhongang Qi, and Ying Shan. T2i-adapter: Learning adapters to dig out more controllable ability for text-to-image diffusion models. In *Proceedings of the AAAI conference on artificial intelligence*, pages 4296–4304, 2024. [6](#), [7](#), [8](#)
- [27] Chong Mou, Xintao Wang, Liangbin Xie, Yanze Wu, Jian Zhang, Zhongang Qi, and Ying Shan. T2i-adapter: Learning adapters to dig out more controllable ability for text-to-image diffusion models. In *Proceedings of the AAAI Conference on Artificial Intelligence*, pages 4296–4304, 2024. [3](#)
- [28] Alexander Quinn Nichol and Prafulla Dhariwal. Improved denoising diffusion probabilistic models. In *International*

Conference on Machine Learning, pages 8162–8171, 2021. 2

[29] Maxime Oquab, Timothée Darcet, Théo Moutakanni, Huy Vo, Marc Szafraniec, Vasil Khalidov, Pierre Fernandez, Daniel Haziza, Francisco Massa, Alaaeldin El-Nouby, et al. Dinov2: Learning robust visual features without supervision. *arXiv preprint arXiv:2304.07193*, 2023. 2, 5, 6, 8, 9

[30] William Peebles and Saining Xie. Scalable diffusion models with transformers. In *Proceedings of the IEEE/CVF International Conference on Computer Vision*, pages 4195–4205, 2023. 2

[31] Dustin Podell, Zion English, Kyle Lacey, Andreas Blattmann, Tim Dockhorn, Jonas Müller, Joe Penna, and Robin Rombach. Sdxl: Improving latent diffusion models for high-resolution image synthesis. *arXiv preprint arXiv:2307.01952*, 2023. 2

[32] Can Qin, Shu Zhang, Ning Yu, Yihao Feng, Xinyi Yang, Yingbo Zhou, Huan Wang, Juan Carlos Niebles, Caiming Xiong, Silvio Savarese, et al. Unicontrol: A unified diffusion model for controllable visual generation in the wild. *arXiv preprint arXiv:2305.11147*, 2023. 1, 3

[33] Yunpeng Qu, Kun Yuan, Jinhua Hao, Kai Zhao, Qizhi Xie, Ming Sun, and Chao Zhou. Visual autoregressive modeling for image super-resolution. *arXiv preprint arXiv:2501.18993*, 2025. 3, 4

[34] Lingmin Ran, Xiaodong Cun, Jia-Wei Liu, Rui Zhao, Song Zijie, Xintao Wang, Jussi Kepo, and Mike Zheng Shou. X-adapter: Adding universal compatibility of plugins for upgraded diffusion model. In *Proceedings of the IEEE/CVF Conference on Computer Vision and Pattern Recognition*, pages 8775–8784, 2024. 3

[35] René Ranftl, Katrin Lasinger, David Hafner, Konrad Schindler, and Vladlen Koltun. Towards robust monocular depth estimation: Mixing datasets for zero-shot cross-dataset transfer. *IEEE transactions on pattern analysis and machine intelligence*, 44(3):1623–1637, 2020. 6

[36] Robin Rombach, Andreas Blattmann, Dominik Lorenz, Patrick Esser, and Björn Ommer. High-resolution image synthesis with latent diffusion models. *Proceedings of the IEEE/CVF Conference on Computer Vision and Pattern Recognition*, pages 10684–10695, 2022. 2

[37] Chitwan Saharia, William Chan, Saurabh Saxena, Lala Li, Jay Whang, Emily L Denton, Kamyar Ghasemipour, Raphael Gontijo Lopes, Burcu Karagol Ayan, Tim Salimans, et al. Photorealistic text-to-image diffusion models with deep language understanding. *Advances in neural information processing systems*, 35:36479–36494, 2022. 2

[38] Tim Salimans, Ian Goodfellow, Wojciech Zaremba, Vicki Cheung, Alec Radford, and Xi Chen. Improved techniques for training gans. *Advances in neural information processing systems*, 29, 2016. 6

[39] Uriel Singer, Adam Polyak, Thomas Hayes, Xi Yin, Jie An, Songyang Zhang, Qiyuan Hu, Harry Yang, Oron Ashual, Oran Gafni, et al. Make-a-video: Text-to-video generation without text-video data. *arXiv preprint arXiv:2209.14792*, 2022. 2

[40] Dan Song, Jian-Hao Zeng, Min Liu, Xuan-Ya Li, and An-An Liu. Fashion customization: Image generation based on editing clue. *IEEE Transactions on Circuits and Systems for Video Technology*, 34(6):4434–4444, 2023. 3

[41] Yang Song, Jascha Sohl-Dickstein, Diederik P Kingma, Abhishek Kumar, Stefano Ermon, and Ben Poole. Score-based generative modeling through stochastic differential equations. *arXiv preprint arXiv:2011.13456*, 2020. 1

[42] Zhuo Su, Wenzhe Liu, Zitong Yu, Dewen Hu, Qing Liao, Qi Tian, Matti Pietikäinen, and Li Liu. Pixel difference networks for efficient edge detection. In *Proceedings of the IEEE/CVF international conference on computer vision*, pages 5117–5127, 2021. 6

[43] Peize Sun, Yi Jiang, Shoufa Chen, Shilong Zhang, Bingyue Peng, Ping Luo, and Zehuan Yuan. Autoregressive model beats diffusion: Llama for scalable image generation. *arXiv preprint arXiv:2406.06525*, 2024. 1, 2

[44] Haotian Tang, Yecheng Wu, Shang Yang, Enze Xie, Junsong Chen, Junyu Chen, Zhuoyang Zhang, Han Cai, Yao Lu, and Song Han. Hart: Efficient visual generation with hybrid autoregressive transformer. *arXiv preprint arXiv:2410.10812*, 2024. 2, 3

[45] Keyu Tian, Yi Jiang, Zehuan Yuan, Bingyue Peng, and Liwei Wang. Visual autoregressive modeling: Scalable image generation via next-scale prediction. *arXiv preprint arXiv:2404.02905*, 2024. 1, 2, 3

[46] Hugo Touvron, Thibaut Lavril, Gautier Izacard, Xavier Martinet, Marie-Anne Lachaux, Timothée Lacroix, Baptiste Rozière, Naman Goyal, Eric Hambro, Faisal Azhar, et al. Llama: Open and efficient foundation language models. *arXiv preprint arXiv:2302.13971*, 2023. 2

[47] Hugo Touvron, Thibaut Lavril, Gautier Izacard, Xavier Martinet, Marie-Anne Lachaux, Timothée Lacroix, Baptiste Rozière, Naman Goyal, Eric Hambro, Faisal Azhar, et al. Llama: Open and efficient foundation language models. *arXiv preprint arXiv:2302.13971*, 2023. 2, 3

[48] Aäron Van Den Oord, Nal Kalchbrenner, and Koray Kavukcuoglu. Pixel recurrent neural networks. In *International conference on machine learning*, pages 1747–1756. PMLR, 2016. 2

[49] Aaron Van Den Oord, Oriol Vinyals, et al. Neural discrete representation learning. *Advances in neural information processing systems*, 30, 2017. 2

[50] Igor Vasiljevic, Nick Kolkin, Shanyi Zhang, Ruotian Luo, Haochen Wang, Falcon Z Dai, Andrea F Daniele, Mohammadreza Mostajabi, Steven Basart, Matthew R Walter, et al. Diode: A dense indoor and outdoor depth dataset. *arXiv preprint arXiv:1908.00463*, 2019. 6

[51] Xin Wang, Yuwei Zhou, Bin Huang, Hong Chen, and Wenwu Zhu. Multi-modal generative ai: Multi-modal llms, diffusions and the unification. *arXiv e-prints*, pages arXiv–2409, 2024. 2

[52] Saining Xie and Zhuowen Tu. Holistically-nested edge detection. In *Proceedings of the IEEE international conference on computer vision*, pages 1395–1403, 2015. 6

[53] Ziyu Yao, Jialin Li, Yifeng Zhou, Yong Liu, Xi Jiang, Chengjie Wang, Feng Zheng, Yuexian Zou, and Lei Li. Car: Controllable autoregressive modeling for visual generation. *arXiv preprint arXiv:2410.04671*, 2024. 2, 3, 4, 6, 7, 8, 9

[54] Dingqiang Ye, Chao Fan, Jingzhe Ma, Xiaoming Liu, and Shiqi Yu. Biggait: Learning gait representation you want by large vision models. In *Proceedings of the IEEE/CVF conference on computer vision and pattern recognition*, pages 200–210, 2024. 8

[55] Dingqiang Ye, Chao Fan, Zhanbo Huang, Chengwen Luo, Jianqiang Li, Shiqi Yu, and Xiaoming Liu. Biggergait: Unlocking gait recognition with layer-wise representations from large vision models. *arXiv preprint arXiv:2505.18132*, 2025. 8

[56] Jianhao Zeng, Dan Song, Weizhi Nie, Hongshuo Tian, Tongtong Wang, and An-An Liu. Cat-dm: Controllable accelerated virtual try-on with diffusion model. In *Proceedings of the IEEE/CVF conference on computer vision and pattern recognition*, pages 8372–8382, 2024. 3

[57] Lvmin Zhang, Anyi Rao, and Maneesh Agrawala. Adding conditional control to text-to-image diffusion models. In *Proceedings of the IEEE/CVF International Conference on Computer Vision*, pages 3836–3847, 2023. 1, 3

[58] Lvmin Zhang, Anyi Rao, and Maneesh Agrawala. Adding conditional control to text-to-image diffusion models. In *Proceedings of the IEEE/CVF international conference on computer vision*, pages 3836–3847, 2023. 6, 7, 8

[59] Nannan Zhang, Yijiang Li, Dong Du, Zheng Chong, Zhengwentai Sun, Jianhao Zeng, Yusheng Dai, Zhengyu Xie, Hairui Zhu, and Xiaoguang Han. Robust-mvton: Learning cross-pose feature alignment and fusion for robust multi-view virtual try-on. In *Proceedings of the Computer Vision and Pattern Recognition Conference*, pages 16029–16039, 2025. 2

[60] Xuanpu Zhang, Dan Song, Pengxin Zhan, Tianyu Chang, Jianhao Zeng, Qingguo Chen, Weihua Luo, and An-An Liu. Boow-vton: Boosting in-the-wild virtual try-on via mask-free pseudo data training. In *Proceedings of the Computer Vision and Pattern Recognition Conference*, pages 26399–26408, 2025. 2

[61] Xiangyu Zhao, Bo Liu, Qijiong Liu, Guangyuan Shi, and Xiao-Ming Wu. Easygen: Easing multimodal generation with bidiffuser and llms. *arXiv preprint arXiv:2310.08949*, 2023. 2

[62] Gaoyue Zhou, Hengkai Pan, Yann LeCun, and Lerrel Pinto. Dino-wm: World models on pre-trained visual features enable zero-shot planning. *arXiv preprint arXiv:2411.04983*, 2024. 2

[63] Xianwei Zhuang, Yuxin Xie, Yufan Deng, Liming Liang, Jinghan Ru, Yuguo Yin, and Yuexian Zou. Vargpt: Unified understanding and generation in a visual autoregressive multimodal large language model, 2025. 2, 3